Single wall carbon nanotubes loaded with Pd and NiPd nanoparticles for H_2 sensing at room temperature

Jaime García-Aguilar, Izaskun Miguel-García, Ángel Berenguer-Murcia[*], *Diego Cazorla-Amorós*

Inorganic Chemistry Department and Materials Science Institute, Alicante University, Ap. 99, E-03080, Alicante, Spain

Pd and bimetallic $Ni_{50}Pd_{50}$ nanoparticles protected by polyvinylpyrrolidone (PVP) have been synthesized by the reduction-by-solvent method and deposited on single wall carbon nanotubes (SWCNTs) to be tested as H_2 sensors. The SWCNTs were deposited by drop casting from different suspensions. The Pd nanoparticles-based sensors show a very reproducible performance with good sensitivity and very low response times (few seconds) for different H_2 concentrations, ranging from 0.2 to 5 % vol. H_2 in air at atmospheric pressure. The influence of the metal nanoparticle composition, the quality of SWCNTs suspension and the metal loading have been studied, observing that all these parameters play an important role in the H_2 sensor performance. Evidence for water formation during the H_2 detection on Pd nanoparticles has been found, and its repercussion on the behaviour of the assembled sensors is discussed.

The sensor preparation procedure detailed in this work has proven to be simple and reproducible to prepare cost-effective and highly efficient H_2 sensors that perform very well under real application conditions.

[*]Corresponding author. Fax: +34 965 903454
E-mail: a.berenguer@ua.es (Á. Berenguer-Murcia)

1. Introduction.

Since the discovery of carbon nanotubes (CNTs) in 1991 by Prof. Iijima [1], a great effort has been made within the scientific community to study their properties and find applications for this allotropic form of carbon. CNTs offer a wide range of interesting properties, such as an unusual electrical conductivity (directly related to their structure), a very high thermal conductivity or exceptional mechanical properties, which make them potential candidates for countless applications like actuators, for gas and energy storage and in field-emitting flat panel displays [2,3,4].

Nowadays the use of H_2 is one of the most promising alternatives to replace fossil fuels in the energy industry. The present energy perspectives focus on the production of H_2 by the electrolysis of water through renewable energy sources and the reforming of hydrocarbons such as ethanol or other organic compounds. However, H_2 is a colourless and odourless gas, with high diffusivity, highly flammable at concentrations above 4% vol., and explosive over a wide range of concentrations (15-59 %) at standard atmospheric pressure. Therefore, safety issues concerning its generation, transport, storage and use must always be considered. There is a wide variety of H_2 sensors capable of measuring different kinds of signals usually based on materials such as optical fibers or semiconductors. Continuous efforts are being made in order to improve sensitivity, selectivity, response time and reliability, as well as diminishing production costs, size and power consumption of the devices, to meet the demands of a future H_2 economy scenario [5]. In this situation, CNTs can be presented as an alternative towards the development of devices designed for the detection of gases including H_2. In this sense, the preparation of CNT-based gas sensors has been widely studied and reported in the literature [6,7].

For the development of gas sensors, a response of the device is required when in the presence of the analyte gas. Among the requirements that these devices must fulfil in order to find a practical application are delivering a stable signal towards the analyte gas under ambient conditions, showing a reversible behaviour, and performing with high sensitivity, selectivity and low response time for different gas concentrations [8]. CNT-based gas sensors have been developed and proved to perform very well for the detection of several analyte gases, such as NH_3, CH_4, H_2S, O_2, NO_2 and H_2 [6,9,10,11].

The main drawback of using CNTs as H_2 sensors is that carbon nanotubes present a weak interaction with the H_2 gas molecules [12,13]. Therefore, for this application, an enhanced interaction between the carbon material and the gas molecules needs to be obtained. One route to achieve this consists in the incorporation of metal nanoparticles which can easily interact with gaseous H_2. In this sense, noble metals such as Pd and Pt are known to readily interact with H_2, chemisorbing the H_2 gas molecules. Among the different metals that can be used for this application, Pd stands as a good option to be included in a H_2 sensor, due to its very good H_2 adsorption and absorption properties and the possibility of forming the metal hydride (PdH_x). The formation of this hydride has been widely reported to be responsible for a very good and reversible performance of the Pd-based H_2 sensors [8,14,15,16]. Pd-based alloys with other metals that present a high affinity for H_2 also appear as a suitable option for these devices, since they would lower the amount of noble metal used and therefore the cost of the device. In this sense, nickel is an interesting metal for this application which has already shown a very good performance in different systems [17,18].

Many of the works regarding this subject reported in the literature use in-situ CVD grown CNTs [19,20], which is a more expensive and substantially more difficult procedure than the use of commercially available CNTs. Often, these works need a purification step of the

CNTs with oxidizing agents, like H_2SO_4 or HNO_3, where the CNTs can be degraded and oxidized [17, 21]. In addition, most of the reports use very difficult and expensive techniques to deposit the metal, such as sputtering, electron beam evaporation or synthesis using dendrimers to link the metal nanoparticles [14,21,22,23]. CNTs suspensions and sensors derived from them can also be found in the literature [24,25]. In these cases, the nanoparticles are generated *in-situ* in the presence of the carbon support, by reducing the metal precursor in the CNTs suspension. The metal loading in these works is found to be around 20% wt. respective to the amount of CNTs used, but the particle size distribution of the metal phase is rather broad, and precise control over the particle size and dispersion of the noble metal phase is not achieved. Furthermore, the influence of the amount and nature of the metal nanoparticles is not analyzed in depth in these works.

In this study we report the preparation of H_2 sensors based on Pd nanoparticle loaded on CNTs by a very simple, low-cost procedure, using commercial Single Wall Carbon Nanotubes (SWCNTs) as support, which are more commonly used for this application rather than Multi Wall Carbon Nanotubes (MWCNTs) due to their relatively better conductive properties. The procedure involves the preparation of the CNTs suspension and the metal nanoparticle suspension separately, and the consecutive deposition of the two suspensions onto a substrate to prepare the sensor. This preparation protocol allows perfect control over the different components in the sensor, including the amount of CNTs and the size, shape and amount of metal deposited on them.

The influence of the amount of metal, the nature of the SWCNTs suspension and the performance of a $Ni_{50}Pd_{50}$ alloy over the sensor response has also been investigated. In addition, reversibility of the samples upon exposure to different atmospheres has also been analyzed, and a possible mechanism responsible for the H_2 detection has been proposed.

2. Experimental.

2.1 Synthesis and purification of the metal nanoparticles

Pure Pd and $Ni_{50}Pd_{50}$ bimetallic nanoparticles were synthetized following the reduction-by-solvent method [26,27]. This method consists in the reduction of the metal precursor by the solvent (which is a diol) in basic media in the presence of a polymer that binds to the metal nanoparticle surface and prevents their agglomeration.

For the bimetallic nanoparticle synthesis, the palladium precursor (Pd acetate, 98 %, Sigma Aldrich) is dissolved in 50 ml of 1,4-dioxane, and the Ni precursor ($NiSO_4 \cdot 6H_2O$, 99 %, Sigma-Aldrich) is dissolved separately at 80ºC for 2 hours in 120 ml of ethylene glycol, using polyvinylpyrrolidone as the capping agent (PVP-40K, Sigma Aldrich). The use of the polymer in this procedure is mandatory to avoid the sintering of the metal nanoparticles once the colloid is formed due to electrostatic interactions, and thus acts as a protecting or capping agent. In this synthesis 1 mmol of metal was used in total and the PVP/Metal molar ratio was set to 10. After complete dissolution, both solutions are mixed at 0 ºC under vigorous stirring, and 1M NaOH is added to adjust the pH to 9. After this step, simultaneous reduction of both metals is started by heating the mixture at 100ºC. The formation of the bimetallic nanoparticles is detected when the solution changes its colour to dark brown. The suspension is then kept at that temperature for 2 hours to ensure complete reduction of the metal precursors. The entire process is carried out under Argon atmosphere by means of a Schlenk system. When the nanoparticles are synthesized it is necessary to do a purification stage in order to remove the excess of polymer and reactants. For the purification, a known volume of nanoparticles (in ethylene glycol) is mixed with

an excess of acetone and stirred vigorously. After a few hours, the nanoparticles flocculate and can be separated from the organic phase that contains the acetone, ethylene glycol and excess of polymer by decantation. Finally, the metal deposit is redispersed in a known amount of methanol so that the final metallic concentration in this solvent is perfectly known. The nanoparticle suspension obtained by this procedure is stable against agglomeration. The pure Pd nanoparticle suspension was prepared using the same experimental procedure, adjusting the Pd amount to the desired concentration.

2.2 Preparation of the SWCNTs suspensions

SWCNTs with an outer diameter of 1-2 nm and a length of 5-30 microns were obtained from Cheap Tubes Inc. (carbon content 97%; purity of the carbon phase: 90 % SWCNT, the other 10 % corresponds to amorphous carbon and MWCNT) and used without further treatment.

Two different SWCNT suspensions were prepared. Suspension 1 (SWCNT-DMF) was prepared using DMF (N, N-dimethylformamide, 99.9 %, Sigma-Aldrich) as solvent. A 30 minutes ultrasonic treatment (SELECTA 3000683) was applied to obtain a homogeneous SWCNT suspension. Suspension 2 (SWCNT-H_2O) was prepared using H_2O as solvent, a surfactant (sodium dodecylbenzenesulfonate (SDBS)), and a polymer (PVP (40K, Sigma Aldrich)), in order to obtain a highly stable suspension, as previously reported by other authors [28]. In both cases, the SWCNT concentration was 0.25 mg/ml.

2.3 Sensors preparation

Sensors were prepared on glass slides (24 x 24 mm, Menzel-Gläser) previously washed with ethanol. Two adhesive copper strips (Copper Conductive Tape, EMS) separated by 2-3 mm were set to serve as connections for the multimeter (6 ½ Digit Multimeter, Agilent). To improve the electrical contact between the CNTs deposit and the copper strips, a layer of silver-epoxy paint (Two-Part Epoxy Adhesive Conductive Silver, EMS) was also applied. 160 µl of the SWCNT suspension were then added between the two copper connections by means of a micropipette to close the electrical circuit. The samples were dried horizontally at 60 ºC for 24 h in an oven. Finally, a known volume of the metal nanoparticle suspension was deposited on the SWCNTs and left to dry at room temperature. Fig. 1 shows a schematic view of the device.

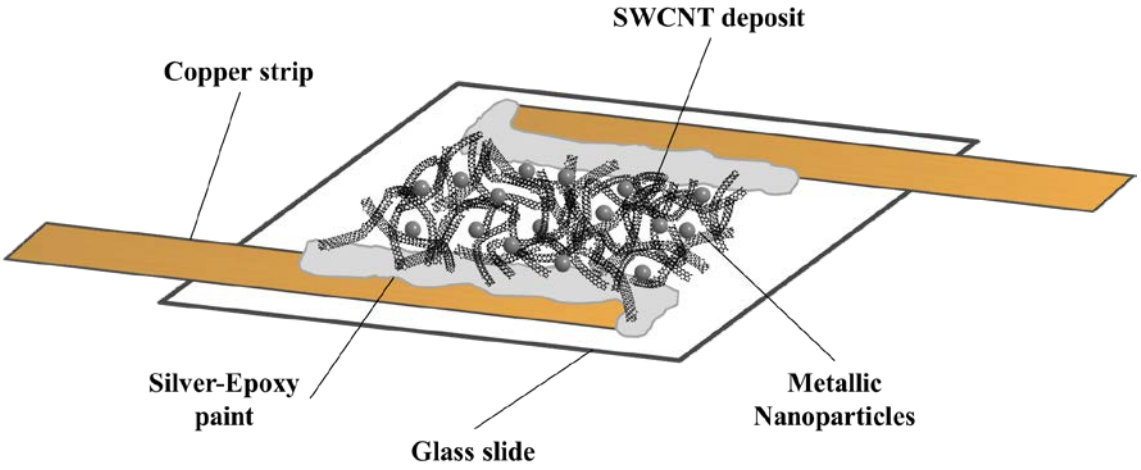

Fig. 1- Scheme of a sample prepared as H_2 sensor.

Table 1 indicates the experimental conditions for the samples prepared for this work, including the amount and metal composition as well as the SWCNTs suspension used in each case.

Table 1. Characteristics of the samples tested as H_2 sensors.

Sample	Suspension	Metal	Metal amount	Metal loading

			(µg)	(wt%)[a]
Pd-DMF	SWCNT-DMF	Pd	10	20
$Ni_{50}Pd_{50}$-DMF	SWCNT-DMF	$Ni_{50}Pd_{50}$	10	20
20-Pd-H_2O	SWCNT-H_2O	Pd	10	20
20-$Ni_{50}Pd_{50}$-H_2O	SWCNT-H_2O	$Ni_{50}Pd_{50}$	10	20
11-Pd-H_2O	SWCNT-H_2O	Pd	5	11

[a] *The metal loading has been calculated from the amount of metal deposited and the SWCNT suspension concentration.*

In addition, other samples have been prepared and tested in H_2 detection experiments. The two SWCNT suspensions prepared, without the addition of metal nanoparticles, were tested as H_2 sensors and no successful results have been obtained. Other experiments using the surfactant (SDBS) and the polymer (PVP) without deposition of SWCNTs yielded the same negative results.

The preparation method of the sensors has been found to be reproducible in terms of SWCNT film thickness, glass area covered and also response of the sensors upon H_2 exposure.

2.4 Samples characterization

The commercial SWCNTs were analyzed by Raman spectroscopy using a LabRam (Jobin-Ivon) equipment operating with a He-Ne laser (632 nm). The SWCNT suspensions were analyzed with a UV-VIS Spectrophotometer (V-670, JASCO) in order to assess the quality of the SWCNT suspensions. Analyses were performed in the 200-1300 nm range, using a quartz cell of 10 mm in length. UV radiation absorption occurs in the SWCNTs around 200-250 nm due to π-electron plasmon formation on their surface. The chemicals used in

the SWCNT-H_2O suspension (PVP and SDBS) also have an absorption in this wavelength interval. For this reason the qualitative measurements were taken at 350 nm.

The metal nanoparticle composition in the samples was characterized by X-ray Photoelectron Spectroscopy (XPS) using a VG-Microtech Multilab 3000 spectrometer, equipped with an Al anode. For the analysis, the SWCNTs were first deposited and then the metal nanoparticles were loaded on them. XPS analyses were performed on the different as-prepared samples and after a treatment in hydrogen simulating a H_2 pulse at room temperature for 4 min as performed in the sensor performance tests (see below). Characterization of the electronic states of each element was made from the relative area of the peak corresponding to each electronic state [29].

The metal composition of the NiPd nanoparticles was analyzed by inductively coupled plasma-optical emission spectroscopy (ICP-OES), in a Perkin-Elmer Optima 4300 system. The extraction of the metal was made by treating the samples with aqua regia at room temperature. The morphology of the sensors was studied by Scanning Electron Microscopy (SEM) using a JEOL JSM-840 equipment. The samples were also characterized by Transmission Electron Microscopy (TEM) coupled to EDX with a JEOL JEM-2010 microscope operating at 200 kV with a space resolution of 0.24 nm. For the analysis, a small amount of the sample was suspended in a few drops of hexane, and sonicated for a few minutes. A drop of this suspension was then deposited onto a 300 mesh Lacey copper grid and left to dry at room temperature. TEM analyses allowed the determination of the metal particle size.

2.5 H_2 Detection tests

The H_2 sensing experiments were performed in a custom-built gas cell connected with stainless steel tubing (1/8” o.d.). For the measurements, the sensors were placed inside a Teflon cell, which was then sealed with a polycarbonate lid and fitted with a Viton O-ring to prevent leaks. A constant gas flow was passed through the cell by means of mass flow controllers (Bronkhorst), while the resistance of the samples was monitored simultaneously with a multimeter (6 ½ Digit Multimeter, Agilent). For all the samples tested, a decrease in the resistance of the sensors has been detected when H_2 is dosed. The outlet of the cell was coupled to a mass spectrometer (Pfeiffer Vacuum, Thermostar) so that the gases coming out of the cell could be analyzed in order to determine the composition of the effluents.

The experiments were performed at room temperature and the gas flow rate was kept constant at 90 ml/min. For a standard H_2 sensing test, a constant flow of synthetic air was flown through the cell until a stable resistance signal was reached. When the signal remained constant, the gas flow was switched to H_2 with a concentration of 3.3 % vol. in air for 4 minutes. After each gas switch, the stream was switched back to synthetic air for 25 minutes in order to completely purge the cell. Additional experiments were also performed at different H_2 concentrations (using synthetic air as carrier gas) in order to evaluate the sensitivity of the sensor. In order to obtain reproducible resistance measurements, a conditioning step of the sensors consisting of three consecutive H_2 switches was carried out. All the results correspond to samples that were submitted to this preliminary conditioning step unless stated otherwise.

Different tests were carried out using N_2 as carrier gas in order to determine the role of oxygen on the sensor performance. In this case, both the stabilization stage and the experiments under H_2 (3.3 % vol.) occur in a N_2 stream.

The sensitivity of the sensor (ΔR) was calculated according to the following equation:

$$|\Delta R| = \frac{|R_H - R_O|}{R_O} \times 100$$

where R_H is the resistance of the sample at a given time and R_O is the initial resistance before each H_2 switch.

The performance as sensors of the prepared materials has also been evaluated by the analysis of two crucial parameters, such as the response time and recovery time [5]. The response time as presented in this study has been defined by previous authors as the time needed by the sensor to reach a resistance value of e^{-1} (36.8 % of the maximum signal measured under the described experimental conditions) [21]. Likewise, the recovery time analyzed in our work has been defined as the time that the sensor needs for the measured signal to reach the R*o* value after the H_2 switch [24]. It should be mentioned, for the sake of clarity towards critical comparison of the results, that other authors [25] define the response time of the sensor as the time taken for the resistance to change from its initial value to 90% of the highest measured value, while the recovery time is defined as the time taken for the resistance to decrease to 10% of the highest measured value.

3. Results and discussion.

The pristine SWCNTs were analyzed by Raman Spectroscopy, obtaining that the sample was composed primarily by semiconducting SWCNTs [30]. The results show that there is a very intense band at ~1570 cm^{-1} corresponding to the G-band typical of semiconducting SWCNTs. Furthermore, the appearance of a band at 2600 cm^{-1} corresponding to the G'-band, the D-band associated to structural defects at 1300 cm^{-1} (with low intensity) and the Radial Breathing Modes (RBM) between 150-300 cm^{-1} can be observed (results not shown).

3.1 SWCNT suspensions characterization

Identical suspensions of SWCNTs were prepared using two different solvents (SWCNT-DMF and SWCNT-H_2O) after undergoing the same aforementioned preparation conditions, i.e. drying temperature, SWCNT concentration, time and volume of SWCNT suspension. Fig. 2 shows the SEM images obtained for each suspension after drop-casting them on a glass slide and recovering the sample for analysis.

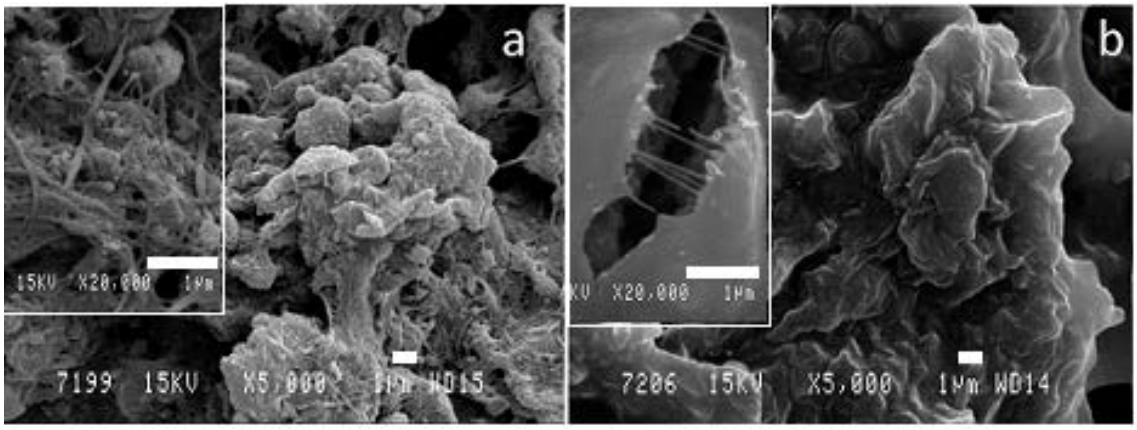

Fig. 2 - SEM images of the a) SWCNT-DMF and b) SWCNT-H_2O suspensions.

Fig. 2a shows the SWCNT from the suspension in DMF, where the SWCNTs are entangled without any apparent order. In the inset of Fig. 2a it is possible to see a magnification of these disordered SWCNTs. The suspension shown in Fig. 2b was prepared using water as solvent, a surfactant and a polymer (SDBS and PVP, respectively) in order to improve the dispersion of SWCNT (SWCNT-H_2O). The mass ratio between CNTs and these two chemicals is ~1/45. As a result of the large amount of polymer present in the suspension, only a polymer matrix can be seen in the micrograph. This sample was submitted to a thermal treatment in air at 350ºC, and the inset in Fig. 2b shows that, although the heat treatment does not successfully remove the polymer or the surfactant from the sample, the SWCNTs can be identified as thin filaments embedded in

the polymer matrix. Although these images correspond to the suspensions drop cast on the glass supports, the same SEM results would be expected for the metal loaded gas sensors.

UV-VIS analyses of these samples indicated that the SWCNT-H_2O suspension shows a much higher UV absorption than the SWCNT-DMF suspension at 350 nm (results not shown). Considering that both DMF and H_2O suspensions were prepared with the same initial concentration (0.25 mg/ml) and that they were analyzed immediately after sonication, the higher absorption band observed for the H_2O sample indicates that in this case, a higher degree of dispersion of the SWCNT is obtained due to the presence of SDBS and PVP [31].

Fig. 3 shows the TEM images of samples SWCNT-H_2O and SWCNT-DMF. Fig. 3a corresponds to SWCNT-H_2O suspension where the SWCNTs can be seen embedded in the polymeric matrix that is seen in the image as an amorphous deposit over the nanotube structure. The inset of this figure shows a bundle of SWCNTs forming groups of 2 to 10 nanotubes. As it has been previously published, the SWCNT suspensions prepared by this methodology allow the preparation of oriented parallel groups of nanotubes that can have a length of up to 1 cm [28]. The possible explanation for this phenomenon is that nanotubes are dispersed in the polymeric matrix, and the SDBS/PVP-SWCNT composite behaves as a liquid crystal system, that generates the formation of oriented arrays. On the other hand, Fig. 3b, shows a deposit of SWCNT-DMF suspension. In this image the SWCNTs can be observed forming a large agglomerate. The dark spots observed in the image within the deposit correspond to cobalt nanoparticles used in the SWCNT synthesis, according to EDX analysis.

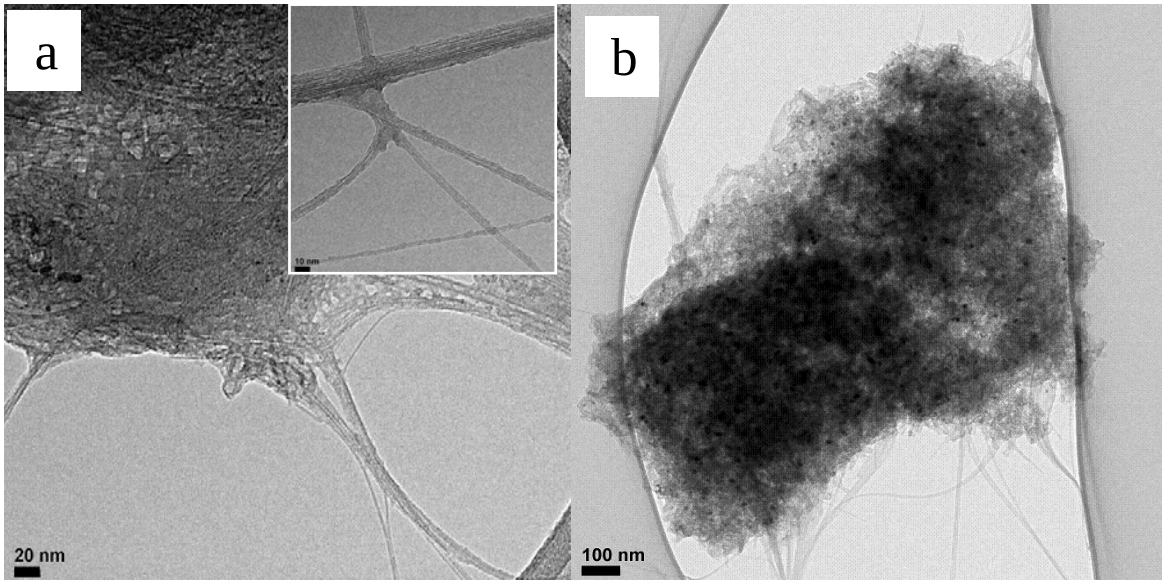

Fig. 3 - TEM images of SWCNTs from the a) SWCNT-H_2O suspension and b) SWCNT-DMF suspension. Inset scale bar: 10 nm.

3.2 Nanoparticles characterization

Fig. 4 shows two representative TEM images corresponding to the samples 20-$Ni_{50}Pd_{50}$-H_2O and $Ni_{50}Pd_{50}$-DMF, which were prepared by drop-casting the SWCNT suspension followed by the corresponding nanoparticle dispersion on a glass slide, followed by recovery of the sample in order to deposit it on a copper TEM grid. The other metal containing materials have similar TEM images. In both samples, the metallic nanoparticles can be seen over the SWCNT deposit and, for that prepared from the H_2O suspension, also inside the polymer matrix (Fig. 4a). The nanoparticles display an average particle size of 2-3 nm, independently of their composition, with a very narrow particle size distribution (results not shown). In addition, a very good dispersion of the particles on the supports with no observable sintering was detected. Therefore, according to our results, the metal dispersion is similar in both samples, and is not affected by the composition of the nanoparticles or the nature of the metal precursors. The larger (≈10 nm) nanoparticles

observed in Figure 4b correspond to the Cobalt catalyst employed for the SWCNT growth by the manufacturer.

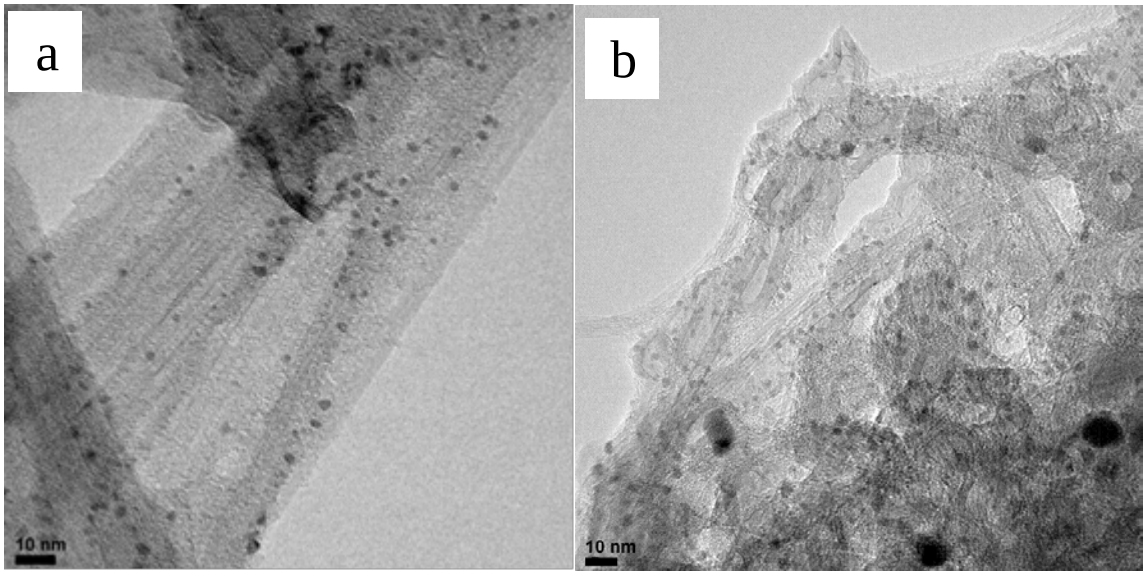

Fig. 4 - TEM images of the nanoparticles in samples a) 20-$Ni_{50}Pd_{50}$-H_2O and b) $Ni_{50}Pd_{50}$-DMF.

The $Ni_{50}Pd_{50}$ nanoparticle composition was also analyzed by ICP-OES and Energy Dispersive X-ray Spectrometry (EDX) and both techniques confirmed an equimolar Ni/Pd ratio, as expected from the synthesis [26]. The elemental analysis of the samples shows that nitrogen has an almost negligible signal for the pure SWCNTs, while in the samples on which metal nanoparticles have been deposited (both for the monometallic and bimetallic nanoparticles), the amount of nitrogen is considerably higher. This indicates that the capping agent used in the synthesis of the nanoparticles (PVP), which contains nitrogen in its structure, is still surrounding the nanoparticle surface after preparation of the sensors. The high amount of nitrogen detected in these samples was not due to remaining DMF, since the SWCNTs analyzed have also been suspended in the same solvent prior to analysis.

The Pd and $Ni_{50}Pd_{50}$ nanoparticles supported over SWCNTs were also characterized by XPS. The samples were analyzed under two different conditions. First, XPS measurements were performed on the as-synthesized sensors (fresh sample) and second, XPS characterization of the samples was performed after a treatment in H_2 at room temperature (reduced samples) which simulated the conditions in which H_2 is passed through the sensor module, in order to check whether the presence of H_2 modifies the chemical properties of the sensors.

Fig. 5 shows the Pd(3d) and Ni(2p) XPS spectra of the sample $Ni_{50}Pd_{50}$-DMF after undergoing a treatment in a H_2 atmosphere identical to that applied in the cell used for the sensor performance measurements. In the Pd spectrum, two peaks can be seen corresponding to the $3d_{5/2}$ and $3d_{3/2}$ transitions, which can be each deconvoluted into two different peaks. Reviewing the literature [25,32] the signals at 335.8eV and 341.2eV correspond to palladium in the metallic state, while the peaks at 337.7eV and 342.2eV correspond to palladium in oxidized species. In the Ni($2p_{3/2}$) XPS, three peaks appear at 856.2 eV, 857.4 eV and 862.3 eV. The large peak situated at 862.3 eV corresponds to a typical Ni satellite peak due to multielectron excitation of this level, whereas the other two correspond to different Ni species.

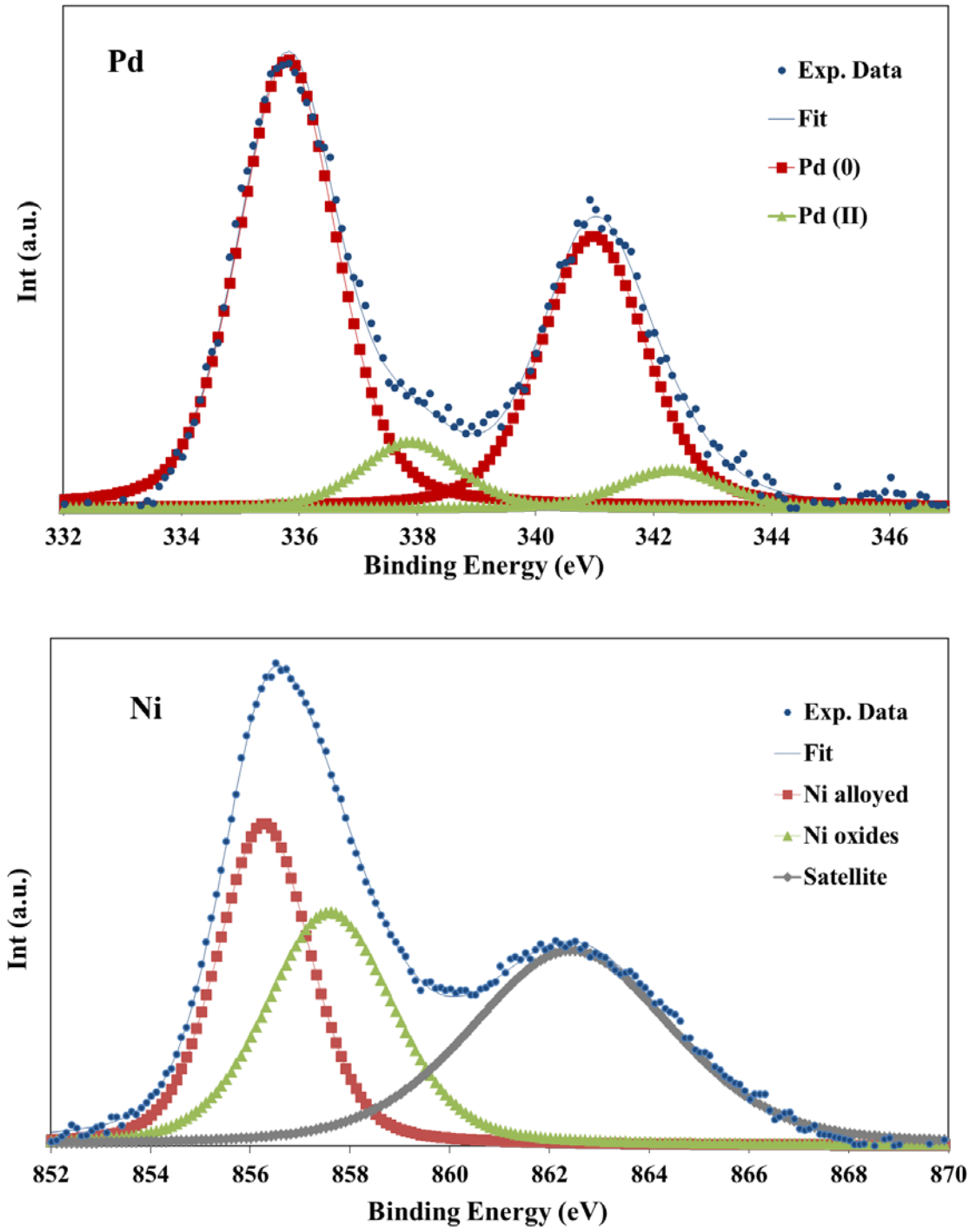

Fig. 5 - XPS spectra of the Pd(3d) and Ni($2p_{3/2}$) transitions in the $Ni_{50}Pd_{50}$-DMF reduced sample.

The XPS analyses of the SWCNTs and the different Pd and $Ni_{50}Pd_{50}$ sensors are shown in Table 2.

Table 2. XPS results of the different samples.

Sample	% Palladium		% Nickel	
	Pd (0)	Pd (II)	Ni (0)	Ni (II)
Pd-DMF (fresh sample)	79.9	20.1	-	-
Pd-DMF (reduced sample)	82.1	17.9	-	-
$Ni_{50}Pd_{50}$-DMF (fresh sample)	81.4	18.6	30.5	69.5
$Ni_{50}Pd_{50}$-DMF (reduced sample)	89.7	10.3	50.7	49.3

For the pure Pd nanoparticles based sensor (fresh sample), some oxidation of the nanoparticles has been detected. This is mainly due to two reasons. On the one hand, it is due to the presence of PVP which, as it has been previously described [33] interacts with the metal nanoparticles withdrawing electron density from their surface and thus generating an electron deficient Pd surface. On the other hand, some surface oxidation due to atmospheric contact of the samples cannot be ruled out. Incomplete reduction of the metal precursor during the nanoparticle synthesis is not responsible for this partial metal oxidation, since H_2 treatment at 200ºC for these nanoparticles does not yield pure Pd(0) nanoparticles, as we have previously reported [27]. When this sample is submitted to a treatment in hydrogen, a slight increase of the amount of metallic Pd is observed (Table 2). As we have previously reported, due to the presence of PVP, complete reduction of the metal of the sample cannot be achieved [27].

For the $Ni_{50}Pd_{50}$ based sensors, important conclusions can be obtained from the XPS data. On the one hand, a significant amount of Ni was detected on the bimetallic nanoparticles. From these results, a Ni:Pd molar ratio of 3:1 is obtained. However, our ICP-OES and EDX results indicated that under the synthesis conditions, nanoparticles with the desired metal composition can be obtained (1:1 metal ratio), in good agreement with what was

previously reported by other authors [26, 34]. Since XPS is a surface characterization technique that provides information from the surface of the materials, and taking into account that the average particle size of the nanoparticles in the sample is in the order of a few nanometers, only surface characterization of the nanoparticles is possible by this technique. We should recall at this point that the metal nanoparticles contain a PVP layer on their surface (whose thickness is not possible to estimate) that the electrons in the XPS chamber must also penetrate in order to reach the nanoparticle surface. Thus, considering the penetration depth of our experimental set-up (around 1 nm) and the size of our polymer-protected nanoparticles, we do not obtain information of the bulk of the particles but mainly of the most external atomic layers of the nanoparticles. Therefore, from our results it can be extracted that, although the bimetallic nanoparticles were synthesized to prepare a homogeneous alloy of the two metals ($Ni_{50}Pd_{50}$), the Ni lies preferentially on the surface of the nanoparticles, whereas the Pd is located in the core of the structure. Therefore, some phase segregation in the nanoparticles (with Ni moving towards the surface of the nanoparticles) might be inferred.

On the other hand, the Ni present in these samples shows a relatively high degree of oxidation, as it can be seen from the binding energies obtained in the spectrum (Fig. 4), where the peaks corresponding to the different Ni species appear at binding energy values significantly higher than those found in the literature [32,35]. This increase of the binding energy suggests that the Ni in these nanoparticles shows some electronic deficient character. The reasons for this could be attributed to the formation of the NiPd alloy since, as it can be observed in Table 2, when the alloy is formed the amount of Pd(0) detected in the fresh sample is higher (81.4 %) than that obtained for the pure Pd sample (79.9 %). This is because when the alloy is generated, Pd interacts with the Ni atoms withdrawing some electronic density from them (due to its higher electronegativity) thus generating

electron deficient Ni species. In addition, there is some degree of interaction between the Ni nanoparticles and the PVP polymer, that would have the same effect on the metal surface as the Pd-PVP interaction [33,36]. Some metal oxidation due to air contact must be also taken into account. After the reduction treatment of sample $Ni_{50}Pd_{50}$-DMF, a significant increase (8 %) of Pd(0) is observed compared with the sample Pd-DMF. This higher degree of Pd reduction in this case is due to higher amount of alloyed Ni (~50 %) and the electronic interaction between the two metals in the bimetallic alloy.

The samples prepared from the SWCNT-H_2O suspension were also characterized by XPS. However, the results are not shown in Table 2 because it was not possible to identify the presence of metal in these samples by this technique. The reason for this might be that the nanoparticles are embedded in the polymer matrix. This could be due to a possible swelling process of the polymer due to interaction or partial dissolution in the methanol used as solvent in the nanoparticle suspensions, which could favour the migration of the nanoparticles into the polymer matrix. Therefore, due to the high amount of polymer contained in the samples, the nanoparticles would not be detected by XPS. However, the presence of the metal nanoparticles is confirmed from the ICP-OES analysis and the TEM observations (see Figure 4a as an example).

3.3 Results of the H_2 detection tests

3.3.1 Tests in synthetic air

The different aforementioned samples were tested as H_2 sensors. It should be mentioned that SWCNT tested as sensors from the H_2O and DMF suspensions (SWCNT-H_2O and

SWCNT-DMF) without the loading of metal nanoparticles did not show any response in the H_2 detection tests, indicating that Co impurities in the SWCNT are not responsible for the sensor response in any case (results not shown). Fig. 6 shows the results of samples tested as H_2 sensors under an air stream.

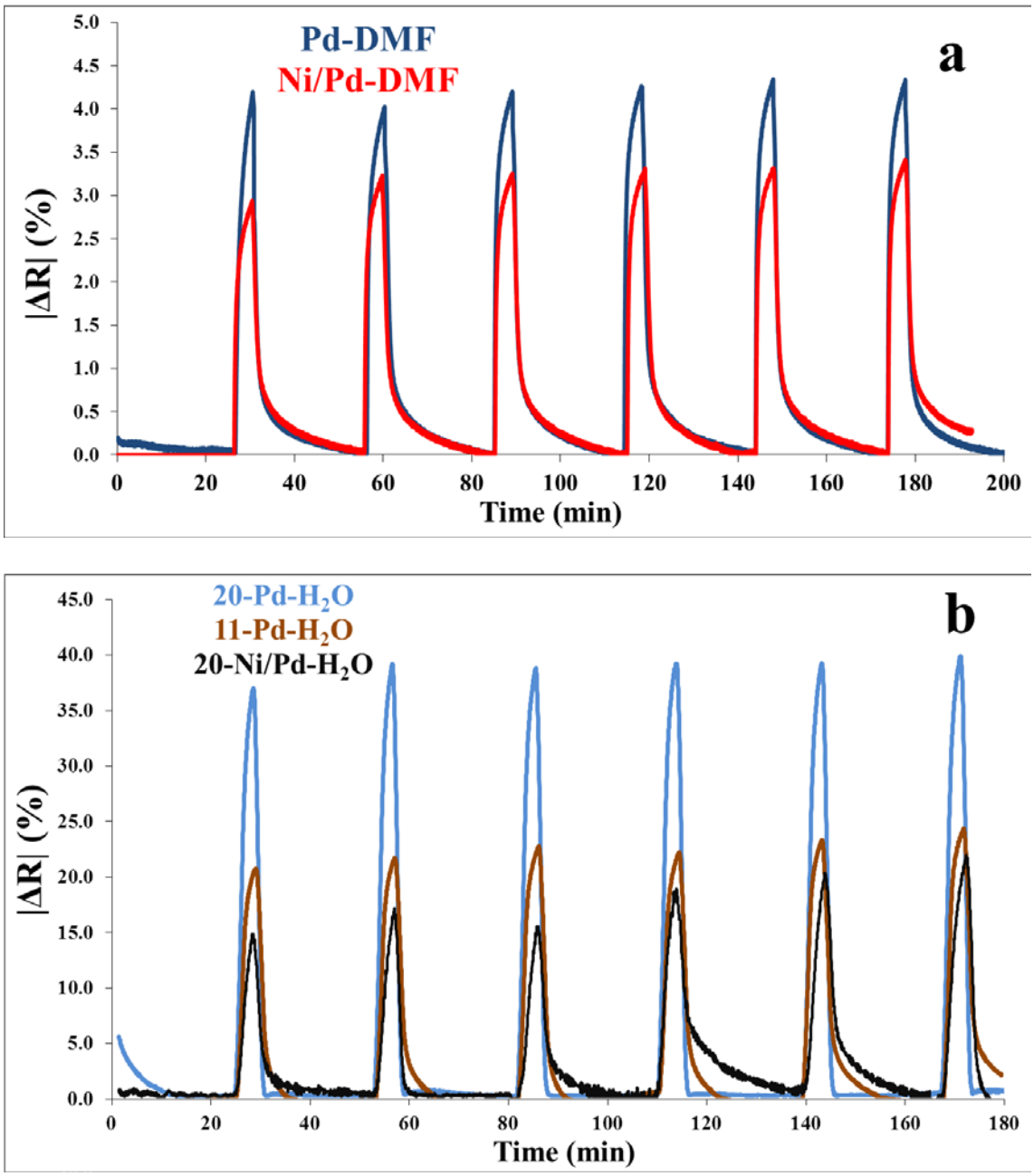

Fig. 6 - Hydrogen detection tests using 3.3 % vol. H_2 in air for the samples prepared from the DMF suspension (a) and the H_2O suspension (b).

A similar behaviour for all the samples (containing metal nanoparticles) can be observed. When H_2 is included in the gas stream, a fast change in the resistance of the sample occurs. When H_2 is removed from the gas stream and synthetic air is flown through the cell, the resistance of the sample recovers its initial value. For all the samples analyzed, the response time has been found to be less than 3 minutes, with the best sample (20-Pd-H_2O) showing a response time of 20 seconds (see below). The recovery time varies depending on the nature of the sample (i.e. nanoparticle composition and metal amount), being below 20 minutes for all the samples tested, and with a value of around 140 seconds (see below) for the sample showing the best performance (20-Pd-H_2O). In addition, a highly stable and reproducible response of all the samples has been obtained for at least 6 consecutive H_2 switches (of the same concentration) over a period of time of at least 3 hours. Relative standard deviation of the resistance signal has been calculated to be 2-3% for all the sensors, excepting sample 20-Ni/Pd-H_2O where slightly higher changes in the resistance have been found.

Significant differences can be also observed from these results. On the one hand, the solvent used for the SWCNT suspension has an outstanding influence over the behaviour of the sensors prepared. When DMF is used as dispersing solvent, maximum resistance changes of ~4 % are obtained in the samples. However, if H_2O is used as solvent, the resistance change of the sample with the same metal loading increases up to 40 % upon H_2 exposure for the best sensor reported in this work (20-Pd-H_2O). The reason for this might be related to the degree of dispersion of the SWCNTs in the different suspensions. Whereas the SWCNTs in DMF give rise to disordered structures with entangled SWCNTs, when H_2O is used as solvent, the CNTs may distribute in more dispersed bundles. In the latter case, the more organized structure of the SWCNTs and the better contact between

the different parts of the device (especially between the SWCNTs and the Pd nanoparticles) might be responsible for an enhanced electrical conductivity of the system, thus improving the sensor response.

Another feature of these samples that may also be highlighted is that using the $Ni_{50}Pd_{50}$ alloy as the active phase does not improve the sensor response. In fact, when Ni is included in the nanoparticle structure, lower resistance increments are obtained for the two prepared suspensions. The reason for this might be because, according to the XPS results, Ni lies preferentially on the surface of the nanoparticles, and since the ability of Pd to adsorb and dissociate the H_2 molecule is larger than that of Ni, when the amount of superficial Pd is diminished in the sample, the sensitivity of the sensor also diminishes. Other works related to H_2 sensing have also evidenced the improved performance of Pd with respect to Ni for this application [17], once again remarking that using Ni for this application does not report a substantial benefit to the behaviour of the system.

Finally, the effect of the metal loading on the sensor behaviour was analyzed, using the sample that showed the best performance (20-Pd-H_2O) and reducing the metallic load (11-Pd-H_2O). As it can be observed from Fig. 6b when the amount of metal deposited decreases, so does the sensitivity of the sensor. In fact, a direct relationship between the metal amount and the resistance change can be detected, since for the sample containing twice the amount of metal loading, a two-fold increase in resistance is obtained. For the sample 11-Pd-H_2O the signal increase is approximately 22 %, which is half the response for the 20-Pd-H_2O sample. This result shows the paramount influence of the metal on the sensor performance, and also indicates that the metal nanoparticles are the active phase in the H_2 sensing mechanism.

In view of its promising results, the best material (20-Pd-H_2O) was submitted to further tests. Thus different H_2 concentrations, ranging from 0.2 to 5 % vol. in air were used in order to monitor the sensitivity of the sensor. The results are shown in Fig. 7.

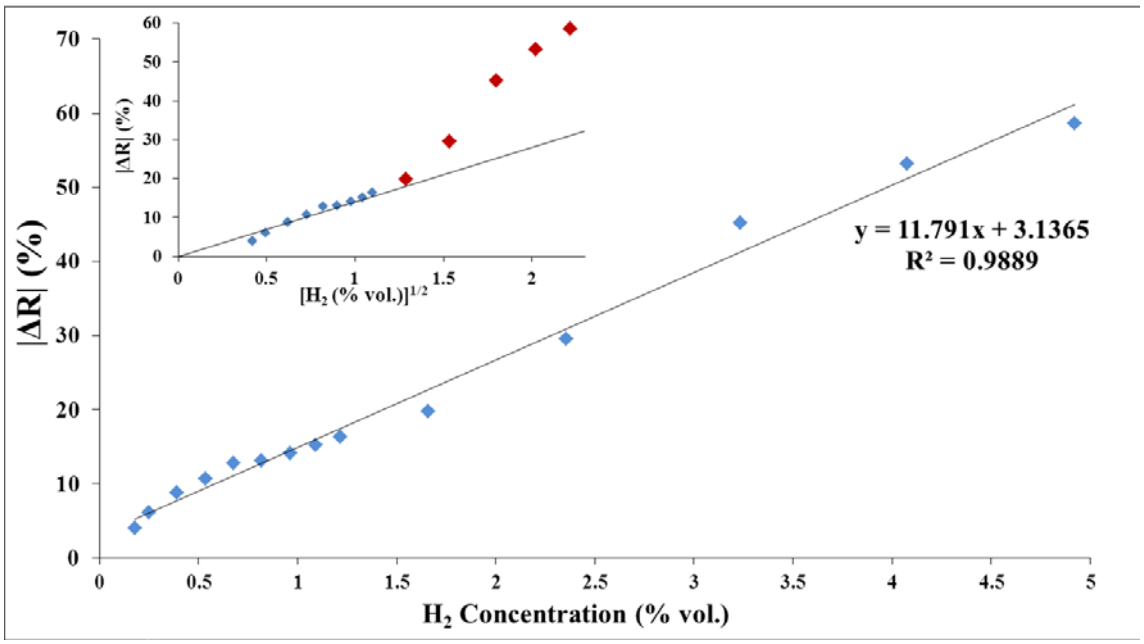

Fig. 7 - Response of the sample 20-Pd-H_2O to different H_2 concentrations. Shown in the inset is the response as a function of the square root of the H_2 concentration (according to Sievert's law). Straight line is a linear fit to data. Red symbols indicate deviation from the linear trend.

As it can be observed, the sample performs with good sensitivity to the different H_2 concentrations in the studied range. The measured resistance increment (|ΔR|) increases with increasing H_2 concentration, which is consistent with general reports. The inset in Fig. 7 shows the response of the sample as a function of the square root of the H_2 concentration. For the lowest gas concentrations (up to 1 % vol. H_2) a linear correlation can be found between these two parameters. This is in good agreement with Sievert's law [37], which describes the equilibrium constant for H_2 dissociative adsorption (at relatively low gas concentrations) [38] on Pd surfaces as a function of the H_2 partial pressure, and explains

gas adsorption on the metal surface as a Langmuir type of behaviour. It is widely accepted that this law is only applicable at H_2 concentrations up to 1 % vol. [37] and experimental data usually deviate from predicted values above that concentration, as is the case of this report.

As explained in the Experimental section, two key parameters which define the performance of a sensor are the response time and recovery time. Fig. 8 shows the response time and the recovery time for sample 20-Pd-H_2O under different H_2 concentrations. As it can be observed, the response time for this sample is always below 1 minute, even for the lowest H_2 concentrations tested. The response time decreases as the H_2 concentration increases, reaching a value of 20 s for concentrations above 0.67 % vol. H_2. The decrease of response time upon increasing the gas concentration is a very common behaviour observed for this kind of devices [14,39]. In addition, the recovery time displayed by the sample is also very low. Although this parameter varies slightly between the different measurements, an average recovery time for this sensor of 140 s (with a minimum value under 120 s) has been measured independently of the H_2 concentration.

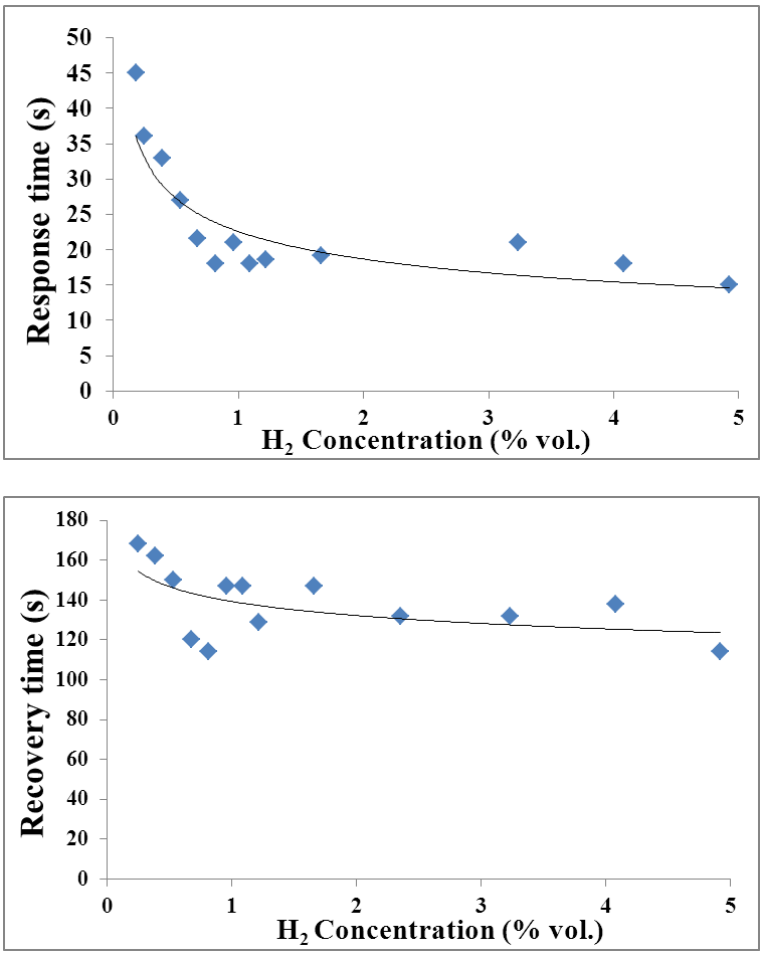

Fig. 8 - Response time and recovery time for sample 20-Pd-H_2O under different H_2 concentrations.

Comparing the results with other Pd based sensors found in the literature, sample 20-Pd-H_2O in this study performs with a higher sensitivity than other systems containing a much higher amount of metal, or prepared by significantly more complex methodologies [14,17 23,24,39]. In addition, the systems presented here also show an enhanced behaviour with respect to similar systems based on multi-wall carbon nanotubes [13, 18].

Response times and recovery times obtained for the samples are in good agreement [17,19,20,21,23] or lower [40] than those found for similar devices in other works.

3.3.2 Role of O_2 in the sensor performance and recovery process.

It is widely accepted that O_2 plays an important role on the system, chiefly in the recovery step of the device [8,17]. In order to understand the detection mechanism in Pd-SWCNT based sensors and to deepen into the influence of molecular O_2 in the sensor behaviour, experiments were performed using N_2 as carrier gas. Fig. 9 shows, as an example, the results of sample 11-Pd-H_2O tested under consecutive switches of 3.3 % vol. H_2/N_2. The same behaviour described here was observed for all the H_2 sensors.

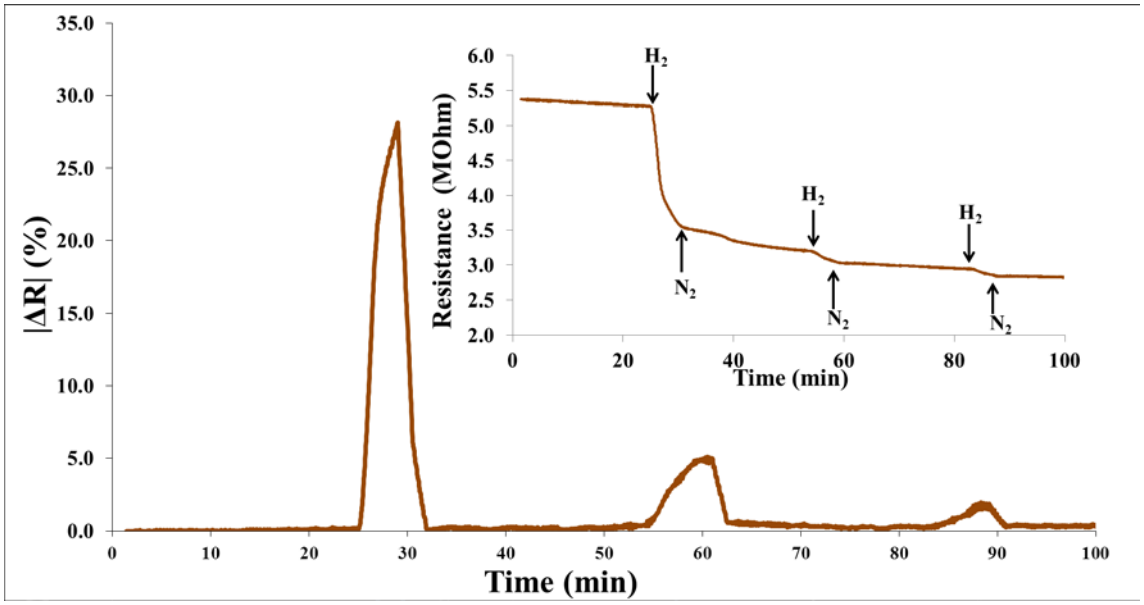

Fig. 9 - Results corresponding to the sample 11-Pd-H_2O tested as H_2 sensor in N_2 atmosphere (3.3 % vol. H_2/N_2). The inset shows the original data of the experiment.

When the sample is submitted to the first H_2 switch in N_2, the sensitivity of the sample is very good and a fast response of the sensor is obtained. However, the response of the sensor diminishes progressively for the next switches, until no resistance change of the sample is obtained upon exposure to H_2. In all the switches, a decrease in resistance is observed (see inset in Figure 9). The decrease in the resistance of the sample in the presence of H_2 has been observed in all the samples prepared for this work both in

presence and absence of oxygen in the gas stream and this response has been widely described in the literature for different kind of systems [16,41,42].

From these experiments carried out in N_2, it can be deduced that the mechanism governing the changes in resistance is one that results in an increase in conductivity. One possibility is that upon adsorption/absorption of H_2 and formation of palladium hydride, the nanoparticle size increases, closing the nanoscopic gaps between the nanoparticles in the sample and therefore diminishing the resistance of the system. On the other hand, when the Pd nanoparticles absorb H_2, the Pd hydride is formed, which is known to have a lower work function than pure Pd, so transfer of electrons to the nanotubes may occur. This, in turn, would reflect as an increase in the resistance of the system considering that the SWCNTs used are mostly p-type semiconductor. Consequently, the observed behaviour of the sensors is the result of the two competitive mechanisms taking place at the same time on the sample. For the sensors prepared in this work, Pd particle size increase upon H_2 exposure enhancing the electrical conductivity of the system, seems to be the main mechanism responsible for the behaviour of the samples (Fig. 10). It must be noted that our proposed mechanism results in a marked decrease in the resistance of the sensing material when it is exposed to a H_2 atmosphere, as evidenced by the different experiments presented in this manuscript. Other authors [43] have recently observed that for a palladium layer deposited by magnetron sputtering on a semiconductor p-type graphene sample the behaviour is the opposite, with the resistance of the system markedly increasing upon exposure to H_2. The authors conclude that the formation of palladium hydride results in an excess electron which is transferred to the graphene support, neutralizing holes in graphene and reducing effective hole concentration in the sample, which causes the electrical conductivity to drop.

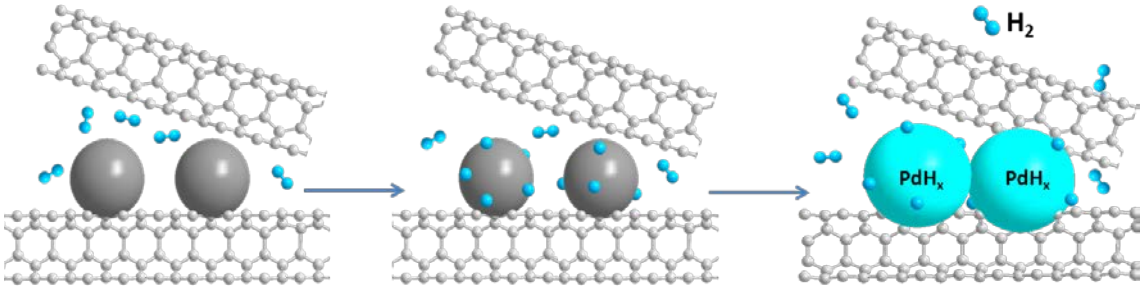

Fig. 10 - Diagram showing the behaviour of the sensor upon H_2 exposure, with an increase in the nanoparticles size and an enhancement of the conductivity of the device.

These experiments also show that the presence of O_2 is essential for a reversible behaviour of the gas sensor, since the recovery of the sensor occurs according to the following reaction: $x/2\ O_2 + PdH_x \rightarrow x/2\ H_2O + Pd$. The absence of gaseous O_2 in the experiment described above is responsible for the much lower sensitivity of the sample in the second and third H_2 switches, with respect to that of the first one. The change of the resistance observed in the second and third H_2 switches could be due to the incomplete formation of the palladium hydride, for this reason the signal intensity decreases with successive switches. Thus, a reversible behaviour of the H_2 sensor in the absence of O_2 is not observed.

Analysis of the gas composition of the stream coming out of the sensing cell by mass spectrometry and when using air as H_2 carrier gas indicated that water is formed on the sensor when H_2 is flown through the cell. Fig. 11 shows the response of the sensor, together with the signals registered by MS spectrometry. As it can be observed, an increase in the H_2O signal (m/z=18) is observed that corresponds perfectly with the H_2 switch (m/z=2) and the decrease of the resistance at the same time. This experimental result evidences the formation of water as a result of the hydrogen oxidation reaction during the H_2 gas switch. Interestingly, the recovery of the resistance after removal of the

H_2 gas, follows the same trend as the H_2O, thus demonstrating that the recovery of the signal is related to hydrogen oxidation and water evolution. The relevance of the water formation reaction on the recuperation stage of the device has been reported in the literature [19].

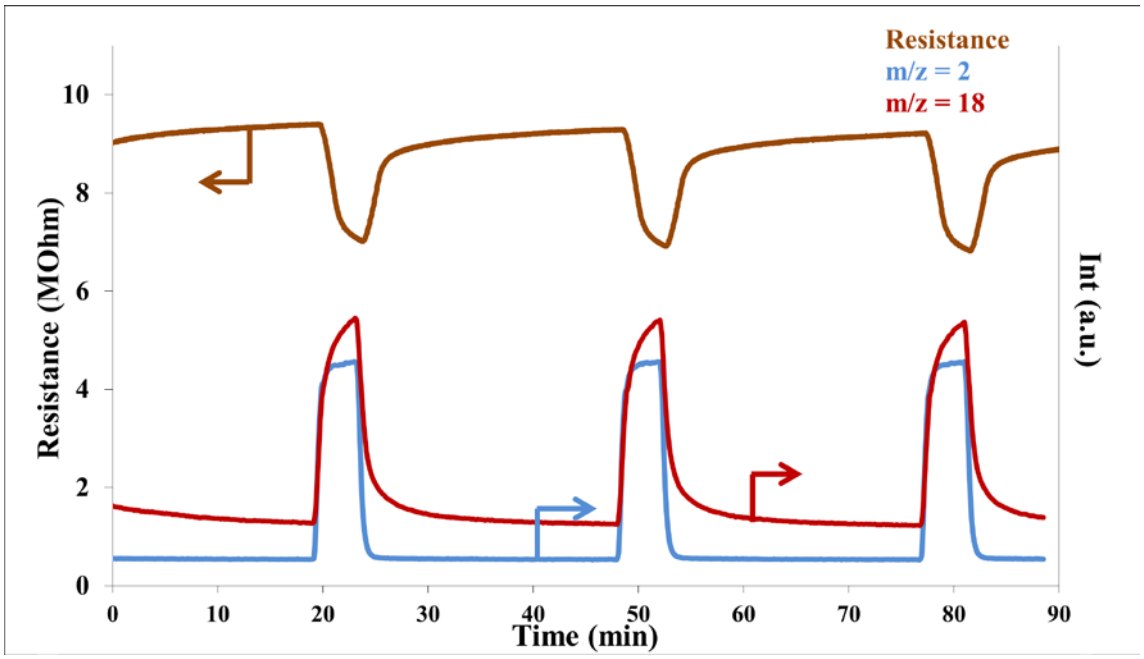

Fig. 11 - Response of sample 11-Pd-H_2O and MS signals obtained in different H_2 switches in air (see Fig. 6b).

Fig. 12 shows a scheme of the two possible processes taking place on the Pd nanoparticle surface during the H_2 sensing process in the presence of O_2. When the sample is exposed to H_2 (Fig 12a) two competing processes can occur. On the one hand, formation of the PdH_x (Fig 12b) and nanogaps closing take place on the nanoparticle surface. On the other hand, O_2 adsorption on the Pd surface (Fig 12c) and subsequent reaction with atomic hydrogen to form water (Fig 12d).

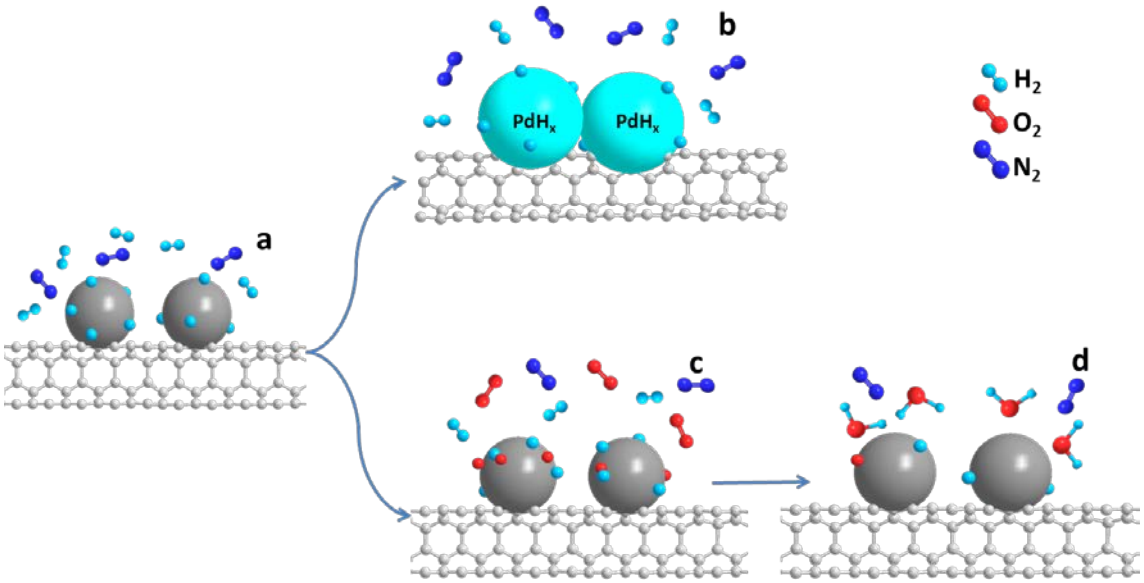

Fig. 12 - Possible processes occurring on the Pd nanoparticles during the H_2 sensing mechanism.

Therefore, according to these results, the process of hydride formation and nanogap closing occurs simultaneously with the water reaction formation on the metal surface. These two mechanisms compete to give rise to the final performance of the sensor which is dominated by the hydride formation according to the observed changes in resistance.

4. Conclusions.

In this work we have prepared H_2 sensors based on SWCNTs with Pd and $Ni_{50}Pd_{50}$ nanoparticles. The method employed to prepare this kind of sensors has proven to be very simple to give rise to highly sensitive sensors which perform with very high reproducibility under realistic conditions. The nature of the suspension of the SWCNT has a paramount influence over the samples behaviour. The sensors prepared from the water suspension show an enhanced sensitivity with respect to DMF-based systems, due to the

higher degree of dispersion of the SWCNTs and the characteristics of the nanoparticle/polymer/SWCNT system.

Alloying of the Pd nanoparticles with Ni diminishes the H_2 response compared to the pure Pd sensors, due to the lower amount of the active metal on the surface. In addition, the amount of metal has an important effect on the sensor performance and higher sensitivities are obtained for the samples with higher metal loading. For the better sample tested, low response times (20 s) and recovery times (140 s) have been measured for H_2 concentrations from 0.2 to 5 % vol. H_2. The presence of O_2 is fundamental for a reversible behaviour of the sensor. Nanoparticles gaps closing upon H_2 exposure has been found to be the main mechanism responsible for the sensing process. However, other physico-chemical reactions do also take place on the nanoparticles surface. Evidences of competitive O_2 adsorption on the metal surface and subsequent water formation have been observed.

Acknowledgements.

We thank the MINECO, Generalitat Valenciana and FEDER (Projects CTQ2012-31762 and PROMETEO/2009/047) for financial support. A.B.M. thanks the Spanish Ministry Science and Innovation for a Ramón y Cajal fellowship (RyC 2009-03913). Jaime Garcia Aguilar and Izaskun Miguel García also thank the University of Alicante for their fellowships.

References

[1] Iijima S. Helical microtubules of graphitic carbon. Nature 1991;354(6348):56-8.

[2] Hu L, Hecht DS, Grüner G. Carbon nanotube thin films: fabrication, properties, and applications. Chem Rev 2010;110(10):5790-844.

[3] Oriňáková R, Oriňák A. Recent applications of carbon nanotubes in hydrogen production and storage. Fuel 2011;90(11):3123-40.

[4] Herrera-Herrera AV, González-Curbelo MÁ, Hernández-Borges J, Rodríguez-Delgado MÁ. Carbon nanotubes applications in separation science: A review. Anal Chim Acta 2012;734:1-30.

[5] Boon-Brett L, Black G, Moretto P, Bousek J A comparison of test methods for the measurement of hydrogen sensor response and recovery times Int J Hydrogen Energ 2010;35:7652-7663.

[6] Kauffman DR, Star A. Carbon nanotube gas and vapor sensors. Angew Chem Int Edit 2008;47(35):6550-70.

[7] Goldoni A, Petaccia L, Lizzit S, Larciprete R. Sensing gases with carbon nanotubes: a review of the actual situation. J Phys-Condens Mat 2010;22(1):013001-8.

[8] Buttner WJ, Post MB, Burgess R, Rivkin C. An overview of hydrogen safety sensors and requirements. Int J Hydrogen Energ 2011;36(3):2462-70.

[9] Kong J, Franklin NR, Zhou C, Chapline MG, Peng S, Cho K, Dai H. Nanotube molecular wires as chemical sensors. Science 2000;287(5453):622-5.

[10] Star A, Joshi V, Skarupo S, Thomas D, Gabriel JCP. Gas sensor array based on metal-decorated carbon nanotubes. J Phys Chem B 2006;110(42):21014-20.

[11] Lu Y, Li J, Han J, Ng HT, Binder C, Partridge C, Meyyappan M. Room temperature methane detection using palladium loaded single-walled carbon nanotube sensors. Chem Phys Lett 2004;391(4):344-8.

[12] Sippel-Oakley J, Wang HT, Kang BS, Wu Z, Ren F, Rinzler AG, Pearton SJ. Carbon nanotube films for room temperature hydrogen sensing. Nanotechnology 2005;16(10):2218-21.

[13] Kumar MK, Ramaprabhu S. Nanostructured Pt functionlized multiwalled carbon nanotube based hydrogen sensor. J Phys Chem B 2006;110(23):11291-8.

[14] Rumiche F, Wang HH, Indacochea JE. Development of a fast-response/high-sensitivity double wall carbon nanotube nanostructured hydrogen sensor. Sensor Actuat B-Chem 2012;163(1):97-106.

[15] Lee J, Shim W, Noh JS, Lee W. Design rules for nanogap-based hydrogen gas sensors. ChemPhysChem 2012;13(6):1395-403.

[16] Favier F, Walter EC, Zach MP, Benter T, Penner RM. Hydrogen sensors and switches from electrodeposited palladium mesowire arrays. Science 2001;293(5538):2227-31.

[17] Lin TC, Huang BR. Palladium nanoparticles modified carbon nanotube/nickel composite rods (Pd/CNT/Ni) for hydrogen sensing. Sensor Actuat B-Chem 2012;162(1):108-13.

[18] Sadek AZ, Zhang C, Hu Z, Partridge JG, McCulloch DG, Wlodarski W, Kalantar-zadeh K. Uniformly dispersed Pt− Ni nanoparticles on nitrogen-doped carbon nanotubes for hydrogen sensing. J Phys Chem C 2010;114(1):238-42.

[19] Sun Y, Wang HH. High-performance, flexible hydrogen sensors that use carbon nanotubes decorated with palladium nanoparticles. Adv Mater 2007;19(19):2818-23.

[20] Kong J, Chapline MG, Dai H. Functionalized carbon nanotubes for molecular hydrogen sensors. Adv Mater 2001;13(18):1384-6.

[21] Ju S, Lee JM, Jung Y, Lee E, Lee W, Kim SJ. Highly sensitive hydrogen gas sensors using single-walled carbon nanotubes grafted with Pd nanoparticles. Sensor Actuat B-Chem 2010;146(1):122-8.

[22] Sayago I, Terrado E, Aleixandre M, Horrillo MC, Fernández MJ, Lozano J, Lafuente E, Maser WK, Benito AM, Martinez MT, Gutiérrez J, Muñoz E. Novel selective sensors based on carbon nanotube films for hydrogen detection. Sensor Actuat B-Chem 2007;122(1):75-80.

[23] Sayago I, Terrado E, Lafuente E, Horrillo MC, Maser WK, Benito AM, Navarro R, Urriolabeitia EP, Martinez MT, Gutierrez J. Hydrogen sensors based on carbon nanotubes thin films. Synthetic Met 2005;148(1):15-9.

[24] Randeniya LK, Martin PJ, Bendavid A. Detection of hydrogen using multi-walled carbon-nanotube yarns coated with nanocrystalline Pd and Pd/Pt layered structures. Carbon 2012;50(5):1786-92.

[25] Kaniyoor A, Ramaprabhu S. Hybrid carbon nanostructured ensembles as chemiresistive hydrogen gas sensors. Carbon 2011;49(1)227-36.

[26] Domínguez-Domínguez S, Berenguer-Murcia Á, Cazorla-Amorós D, Linares-Solano Á. Semihydrogenation of phenylacetylene catalyzed by metallic nanoparticles containing noble metals. J Catal 2006;243(1):74-81.

[27] Miguel-García I, Berenguer-Murcia Á, Cazorla-Amorós D. Preferential oxidation of CO catalyzed by supported polymer-protected palladium-based nanoparticles. Appl Catal B-Environ 2010;98(3-4):161-70.

[28] Bravo-Sanchez M, Simmons TJ, Vidal MA. Liquid crystal behavior of single wall carbon nanotubes. Carbon 2010;48(12):3531-42.

[29] Voogt EH, Mens AJM, Gijzeman OLJ, Geus JW. XPS analysis of palladium oxide layers and particles. Surf Sci 1996;350(1-3):21-31.

[30] Dresselhaus MS, Dresselhaus G, Hofmann M. The big picture of Raman scattering in carbon nanotubes. Vib Spectrosc 2007;45(2):71-81.

[31] Rance GA, Marsh DH, Nicholas RJ, Khlobystov AN. UV-vis absorption spectroscopy of carbon nanotubes: relation between the π-electron plasmon and nanotube diameter. Chem Phys Lett 2010;493(1):19-23.

[32] Park KW, Choi JH, Kwon BK, Lee SA, Sung YE. Chemical and electronic effects of Ni in Pt/Ni and Pt/Ru/Ni alloy nanoparticles in methanol electrooxidation. J Phys Chem B 2002;106(8):1869-77.

[33] Miguel-García I, Berenguer-Murcia Á, García T, Cazorla-Amorós D. Effect of the aging time of PVP coated palladium nanoparticles colloidal suspensions on their catalytic activity in the preferential oxidation of CO. Catal Today 2012;187(1):2-9.

[34] Lu P, Teranishi T, Asakura K, Miyake M, Toshima N. Polymer-protected Ni/Pd bimetallic nano-clusters: preparation, characterization and catalysis for hydrogenation of nitrobenzene. J Phys Chem B 1999;103(44):9673-82.

[35] Singh SK, Iizuka Y, Xu Q. Nickel-palladium nanoparticle catalyzed hydrogen generation from hydrous hydrazine for chemical hydrogen storage. Int J Hydrogen Energ 2011;36(18):11794-801.

[36] Couto GG, Klein JJ, Schreiner WH, Mosca DH, de Oliveira AJA, Zarbin AJG. Nickel nanoparticles obtained by a modified polyol process: Synthesis, characterization, and magnetic properties. J Colloid Interf Sci 2007;311(2):461-8.

[37] Sievert A, Danz, W. Solubility of D_2 and H_2 in Palladium. Z Phys Chem 1936;34:158.

[38] Yang F, Kung SC, Cheng M, Hemminger JC, Penner RM. Smaller is faster and more sensitive: the effect of wire size on the detection of hydrogen by single palladium nanowires. ACS nano 2010;4(9):5233-44.

[39] Ding D, Chen Z, Rajaputra S, Singh V. Hydrogen sensors based on aligned carbon nanotubes in an anodic aluminum oxide template with palladium as a top electrode. Sensor Actuat B-Chem 2007;124(1):12-7.

[40] Mubeen S, Zhang T, Yoo B, Deshusses MA, Myung NV. Palladium nanoparticles decorated single-walled carbon nanotube hydrogen sensor. J Phys Chem C 2007;111(17):6321-7.

[41] Lee J, Shim W, Lee E, Noh J-S, Lee W. Highly mobile palladium thin films on an elastomeric substrate: nanogap-based hydrogen gas sensors. Angew Chem Int Edit 2011;50(23):5301-05.

[42] Im Y, Lee C, Vasquez RP, Bangar MA, Myung NV, Menke EJ, Penner RM, Yun M. Investigation of a single Pd nanowire for use as a hydrogen sensor. Small 2006;2(3):356-8.

[43]Lim, J., Hwang, S., Yoon, H.S., Lee, E., Lee, W., Jun, S.C., Asymmetric electron hole distribution in single-layer graphene for use in hydrogen gas detection, Carbon (2013), doi: http://dx.doi.org/10.1016/j.carbon.2013.05.071